

# Exploring alternative red seaweed species for the production of agar-based hydrogels for food applications

Vera Cebrián-Lloret<sup>a</sup>, Antonio Martínez-Abad<sup>a</sup>, Amparo López-Rubio<sup>a</sup>, Marta Martínez-Sanz<sup>b,\*</sup>

<sup>a</sup> Food Safety and Preservation Department, IATA-CSIC, Avda. Agustín Escardino 7, 46980 Paterna, Valencia, Spain

<sup>b</sup> Instituto de Investigación en Ciencias de la Alimentación (CSIC-UAM, CEI UAM + CSIC), Nicolás Cabrera 9, 28049, Madrid, Spain

## ARTICLE INFO

**Keywords:**  
Seaweeds  
Agar  
Hydrogels  
Gelation  
SAXS

## ABSTRACT

Three different red seaweed species, *Gelidium corneum* and two *Gracilaria* species (*Agarophyton chilensis*, and *Gracilariopsis longissima*), were used to produce agar-based fractions through conventional and simplified extraction methods and their composition and gel-forming properties were evaluated. The use of an alkaline pre-treatment was effective in removing impurities such as proteins, lipids, and ash, while the agarose/agarpectin ratio in agar was not affected. This led to the formation of hydrogels with higher stiffness and strength. Surprisingly, the presence of semi-crystalline agarpectin in the agar fractions from the two *Gracilaria* species, especially *G. longissima*, promoted the formation of more densely packed and stronger hydrogel networks, with higher gelling temperatures and superior mechanical properties. Thus, these results suggest that *G. longissima* has the potential to be used as an alternative to the more widespread use of *G. corneum* for the production of agar hydrogels for food applications.

## 1. Introduction

Thickening and gelling agents play a critical role in the food industry, as they are widely employed to modify the texture and consistency of food products (Qin, Jiang, Zhao, Zhang, & Wang, 2018). These gelling agents are typically hydrocolloids that have the unique ability to bind with water molecules and produce gel-like structures, imparting a desirable texture to the final product (Fathima et al., 2022; Williams & Phillips, 2021, pp. 3–26). The properties of the resulting gels, such as firmness, elasticity, and stability, depend on the type and concentration of the gelling agent used (Cong et al., 2022), as well as the gelling mechanism and parameters affecting the process, such as the temperature, presence of salts, etc. Traditionally, thickening and gelling agents derived from animals, such as gelatine derived from animal bones and skin, have been extensively utilized in the food industry (Williams & Phillips, 2021, pp. 3–26). However, due to the heightened consciousness of animal welfare, the rapid growth of the vegetarian and vegan markets, and consumers' inclination towards healthy and eco-friendly food options, individuals are increasingly willing to modify their habits and assume accountability for climate change by selecting plant-based foods over animal-based alternatives, thereby reducing their carbon footprint (He, Meda, Reaney, & Mustafa, 2021; McClements & Grossmann, 2021;

Williams & Phillips, 2021, pp. 3–26). In this context, marine sources, such as seaweeds or aquatic plants, are being investigated as a potential source of biopolymers with gelling properties (Kartik et al., 2021; Martínez-Sanz, Cebrián-Lloret, Mazarro-Ruiz, & López-Rubio, 2020; Özçimen, Benan, Morkoç, & Efe, 2017, pp. 7–14). In particular, algal cell walls contain a variety of polysaccharides with different functionalities which can be exploited as gelling agents (Kartik et al., 2021). Sulphated polysaccharides, such as carrageenan and agar, are of particular interest to the food industry as they can be used as gelling, thickening, and stabilizing agents (Cebrián-Lloret, Göksen, Martínez-Abad, López-Rubio, & Martínez-Sanz, 2022; Jayakody, Vanniarachchy, & Wijesekara, 2022; Pangestuti & Kim, 2015). Agar, found in the cell walls of some red seaweed species (Rhodophyta), is composed of two main fractions: agarose, the gelling fraction, which consists of alternating units of  $\beta$ -D-galactopyranose and 3,6-anhydro- $\alpha$ -L-galactopyranose, and agarpectin, which presents a structure similar to agarose but may also contain sulphate esters and other residues, such as methoxyl groups and pyruvic acid. The presence of a greater proportion of sulphate groups in agar is frequently related to a reduced gelling ability and it influences gelling temperature and melting behaviour (Cebrián-Lloret, Göksen, et al., 2022; Lee et al., 2017; Martínez-Sanz, Ström, et al., 2020; Yarnpakdee, Benjakul, & Kingwascharapong, 2015). For the extraction of

\* Corresponding author

E-mail address: [marta.martinez@csic.es](mailto:marta.martinez@csic.es) (M. Martínez-Sanz).

<https://doi.org/10.1016/j.foodhyd.2023.109177>

Received 21 June 2023; Received in revised form 3 August 2023; Accepted 15 August 2023

Available online 18 August 2023

0268-005X/© 2023 The Author(s). Published by Elsevier Ltd. This is an open access article under the CC BY-NC-ND license (<http://creativecommons.org/licenses/by-nc-nd/4.0/>).

agar, *Gelidium corneum* (formerly known as *Gelidium sesquipedale*) is the most commonly utilized seaweed species in Spain and Morocco, as it yields agars with higher gelling capacity compared to those obtained from other species, such as *Gracilaria* spp. (Martínez-Sanz, Gómez-Mascaraque, et al., 2019; Rocha et al., 2019; Wang et al., 2017). The industrial-scale extraction of agar involves alkaline pre-treatments, high-temperature and pressure extraction, filtration processes, and freeze-thaw cycles. However, due to the time and energy requirements of this process, efforts are being made to develop more sustainable and energy-efficient extraction protocols. In line with this, simplified methods, reducing the total extraction time and the number of extraction steps, have been proposed to obtain less purified agar fractions, which have shown good antioxidant properties (Cebrián-Lloret, Gökse, et al., 2022; Martínez-Sanz et al., 2021; Martínez-Sanz, Gómez-Mascaraque, et al., 2019). Even if the less purified agar-based fractions may not meet the requirements of high-purity applications (e.g. microbiology applications), they can still be beneficial for other purposes, such as food additives with bioactive properties or food packaging materials (Cebrián-Lloret, Gökse, et al., 2022). Furthermore, for food applications in which high agarose purity is not a requirement, it may also be interesting to explore other seaweed species with more competitive prices than *Gelidium corneum*.

Consequently, three different species of red seaweeds were employed for this study: *Gelidium corneum* (formerly *Gelidium sesquipedale*) and *Agarophyton chilensis* (formerly *Gracilaria chilensis*), which are traditionally used for agar extraction, as well as *Gracilariopsis longissima* (formerly *Gracilaria verrucosa*) which is a species that is not commonly utilized for agar extraction but is cost-effective to cultivate (Bermejo et al., 2020; Mouga & Fernandes, 2022).

The aim of this study was, therefore, to conduct a comparative analysis of the composition of various agar-based fractions produced using two distinct methods: (i) a conventional agar purification process similar to the one commonly used in the industry (including a harsh alkaline pre-treatment followed by extraction with boiling water), and (ii) an alternative simplified extraction protocol that yields less purified agar fractions (omitting the pre-treatment step). In addition, the properties of the gels formed by each of the agar-based fractions have been evaluated to determine their suitability for application in the food industry. This will allow evaluating the potential of producing high-quality agar-based additives through more sustainable processes and using more cost-effective sources.

## 2. Materials and methods

### 2.1. Materials

Hispanagar S.A. (Burgos, Spain) kindly provided the three red seaweed species, *Gelidium corneum*, *Agarophyton chilensis*, and *Gracilariopsis longissima*. Prior to the extraction of agar, the seaweeds were washed with tap water to remove sand and other impurities, dried by means of a Digitronic-TFT oven (J.P. SELECTA, Spain) for 24 h at 50 °C, and ground into fine powder with a particle size of less than 250 µm using a ZM 200 Model Ultra-Centrifugal Mill (Retsch, Germany).

### 2.2. Production of the agar-based extracts

Agar was extracted from the biomass of the three seaweed species by applying a hot water extraction procedure, as well as a pre-treatment purification step, as previously described by Martínez-Sanz et al. (Martínez-Sanz, Gómez-Mascaraque, et al., 2019). The extraction procedure involved immersing 50 g of dry seaweed powder in 500 mL of distilled water, heating to 90 °C for 2 h, and then quickly separating the hot agar-based solution from the solid residue by filtration using a muslin cloth at room temperature. The resulting filtrate was gelled and frozen overnight at −21 °C, followed by two freeze-thaw cycles to improve the elastic properties of the gels, and finally the resulting gel was

freeze-dried using a Lyobeta 6 PL freeze dryer (Telstar, Japan). The so obtained agar-based fractions from *G. corneum*, *A. chilensis*, and *G. longissima* were coded as HW-G, HW-C, and HW-L respectively. In addition, a pre-treatment step was evaluated prior to the extraction process, which involved soaking 50 g of dry seaweed powder in 500 mL of 10% (w/v) NaOH solution, heating to 90 °C for 2 h, filtering using a muslin cloth and washing the solid material with distilled water. The obtained solid was then subjected to the hot water treatment described above. The resulting purified agar fractions were coded as NaOH-G, NaOH-C, and NaOH-L, respectively.

### 2.3. Production of the agar-based dispersions and hydrogels

Freeze-dried agar-based extracts were dispersed in distilled water at a concentration of 2.5% (w/w) by heating at 95 °C for at least 45 min. The resulting hot solutions were then used to fill the rheometer plate or SAXS capillaries. For compression tests, the hot solutions were poured into 18 mm diameter methacrylate moulds and allowed to cool overnight at 25 °C to form disk-like hydrogel specimens.

### 2.4. Compositional analysis

All the determinations were carried out at least in triplicate, as described below.

#### 2.4.1. Carbohydrate analysis

To determine the carbohydrate composition, the methodology established by Stevenson & Furneaux (Quemener & Lahaye, 1998; Stevenson & Furneaux, 1991), with slight modifications, was employed. In brief, 10 mg of dry sample were dissolved in a 5 mL aqueous rhamnose solution (0.5 mg/mL, internal standard) and incubated at 95 °C for 40 min. Subsequently, 0.5 mL of the solution was dried in Pyrex tubes, followed by a pre-hydrolysis step involving the addition of 50 µL of 4-methylmorpholine-borane (MMB) and 200 µL of 3 M trifluoroacetic acid to the tubes, which were then placed in a heat block at 80 °C for 30 min. After cooling, 50 µL of MMB solution were added, and the samples were dried. For the main hydrolysis, 200 µL of 2 M trifluoroacetic acid were added to the tubes, which were then kept at 120 °C in the thermoblock for 1 h. Following this, 100 µL of MMB solution was added, and the samples were dried at 50 °C. After drying, the samples were resuspended in 1 mL H<sub>2</sub>O, filtered through 0.45 µm syringe filters, and transferred to chromatography vials. The monosaccharides were then analysed via high-performance anion-exchange chromatography with pulsed amperometric detection (HPAEC-PAD) on an ICS-6000 (Dionex, ThermoFisher Scientific, Sunnyvale, CA, USA). Control samples containing known concentrations of mixtures of glucose, galactose, rhamnose, 3,6-anhydro-L-galactose, and 6-O-methyl-D-galactose were reduced to their corresponding alditols and used for calibration.

#### 2.4.2. Ash content

To determine the mineral content of the agar-based fractions, the ash content was measured through dry biomass calcination using the standard TAPPI T211 om-07 method. About 0.25 g of dried material was placed into a pre-weighed crucible, which was then weighed. The combustion process was carried out in a muffle furnace at 550 °C for 24 h, after which the ash content was determined through gravimetric quantification.

#### 2.4.3. Lipid content

The Folch method, with slight modifications (Löfgren et al., 2012), was employed to estimate the total lipid content of the samples. In brief, 30 mg of the sample was suspended in 200 µL of MilliQ water and transferred to a 10 mL tube. Subsequently, 1660 µL of methanol was added and mixed at 1400 rpm for 10 min. Next, 3320 µL of dichloromethane was added, and the mixture was stirred at 1400 rpm for 20 min. A solution of 1000 µL of 20 mM acetic acid was added to the tube and

stirred at 1400 rpm for another 10 min. After centrifugation, the lower organic phase was transferred to a new tube, and the aqueous phase was washed with 1660  $\mu\text{L}$  of dichloromethane. This process of centrifugation and phase separation was repeated, and the organic phase was pooled. The content of this tube was then filtered using a glass syringe and a 0.45 nm filter. The organic solvent was evaporated, and the total lipid content was determined gravimetrically.

#### 2.4.4. Protein content

The total nitrogen content of the samples was determined by employing an Elemental Analyzer Rapid N Exceed (Paralab S.L., Spain). To accomplish this, approximately 100 mg of each powdered sample was pressed to form a pellet and subjected to analysis using the Dumas method. This technique is based on the complete and instantaneous oxidation of the sample by combustion with oxygen at a temperature of approximately 1020 °C. The combustion products are transported by the carrier gas to a chromatographic column where the separation takes place. A thermal conductivity detector provides the signal for  $\text{N}_2$  which is translated into percentage content. (Wiles, Gray, & Kissling, 1998). The total protein content was then estimated by multiplying the nitrogen content by a factor of 6.25.

#### 2.4.5. Total phenolic content

To determine the total phenolic content of the agar-based fractions, the Folin-Ciocalteu method (Singleton, Orthofer, & Lamuela-Raventós, 1999) was employed. The dry samples were dissolved in water at a concentration of 5 mg/mL. A colorimetric assay was performed by mixing 125  $\mu\text{L}$  of a 1:10 dilution of Folin-Ciocalteu reagent with 20  $\mu\text{L}$  of the sample. Next, 100  $\mu\text{L}$  of sodium carbonate (75 mg/mL) were added and the samples were heated at 40 °C for 10 min. Absorbance values were measured at a wavelength of 750 nm, and a calibration curve was constructed using gallic acid as a standard. The total phenolic content was expressed as mg of gallic acid (GA)/g extract.

#### 2.4.6. Sulphate content

The sulphur content of the samples was determined using a Flash Smart™ Elemental Analyzer (ThermoFisher, Massachusetts, USA). To this purpose, the samples underwent a complete and instantaneous oxidation through combustion with oxygen at an approximate temperature of 1020 °C.

### 2.5. $\text{ABTS}^{\cdot+}$ radical cation scavenging activity

The agar-based extracts were evaluated for their ability to scavenge the  $\text{ABTS}^{\cdot+}$  radical cation, as per the methodology described by Re et al. (Re et al., 1999). In summary, 0.192 g of ABTS was dissolved in 50 mL of PBS at pH 7.4 and combined with 0.033 g of potassium persulphate to generate the  $\text{ABTS}^{\cdot+}$  radical cation, which was left to incubate in the dark overnight. Prior to the assay, the  $\text{ABTS}^{\cdot+}$  solution was diluted with PBS to obtain an initial absorbance of  $\sim 0.700 \pm 0.02$  at 734 nm and room temperature. The radical scavenging activity of the agar-based extracts was measured by mixing 230  $\mu\text{L}$  of the diluted  $\text{ABTS}^{\cdot+}$  solution with 20  $\mu\text{L}$  of each sample and observing the change in absorbance after 6 min. The antioxidant capacity of the extracts was calculated in mg Trolox equivalents (TE)/g extract, using a calibration curve obtained with 6-hydroxy-2,5,7,8-tetramethylchromane-2-carboxylic acid (Trolox).

### 2.6. Fourier transform infrared spectroscopy (FT-IR)

The agar-based fractions were analysed using FT-IR in attenuated total reflectance (ATR) mode, utilizing a Jasco FT/IR-4100 (Easton, USA) instrument. Spectra were recorded with a resolution of 4  $\text{cm}^{-1}$ , covering a wavelength range from 400 to 4000  $\text{cm}^{-1}$ , and an average of at least 32 scans was obtained for each measurement.

### 2.7. Small Angle X-ray scattering (SAXS) experiments

Small Angle X-Ray Scattering (SAXS) experiments were conducted at the Non-Crystalline Diffraction beamline (BL-11) from the ALBA synchrotron light source. The different agar-based aqueous dispersions were placed into 2 mm quartz capillaries (Hilgenburg GmbH, Germany) and left at room temperature for at least 24 h to form the gels inside the capillaries, which were then sealed for analysis. The incident photons had an energy of 12.4 keV or a wavelength of  $\lambda = 1 \text{ \AA}$ . The SAXS diffraction patterns were collected using a Pilatus 1 M photon counting detector, which had an active area of  $168.7 \times 179.4 \text{ mm}^2$ , an effective pixel size of  $172 \times 172 \text{ }\mu\text{m}^2$ , and a dynamic range of 20 bits. The sample-to-detector distance was set at 6570 mm, providing a  $q$  range with a maximum value of  $q = 0.2 \text{ \AA}^{-1}$ . Preliminary trials were conducted to determine an appropriate exposure time of 5 s. The pyFAI python code (ESRF) (Kieffer & Wright, 2013), modified by the ALBA beamline staff, was used for online azimuthal integrations from a previously calibrated file, with the calibration files created from a silver behenate standard. The radially averaged intensity profiles were then plotted as a function of  $q$  using the IRENA macro suite (Ilavsky & Jemian, 2009) within the Igor software package (Wavemetrics, Lake Oswego, Oregon).

The experimental data were fitted using either a correlation length model or a two-level unified model. The correlation length model contains a first term, described by a power-law function, which accounts for the scattering from large clusters in the low  $q$  region and a second term, consisting of a Lorentzian function, which describes scattering from polymer chains in the high  $q$  region:

$$I(q) = \frac{A}{q^n} + \frac{C}{1 + (q\xi_L)^m} + bkg \quad (1)$$

where  $n$  is the power-law exponent,  $A$  is the power-law coefficient,  $m$  is the Lorentzian exponent,  $C$  is the Lorentzian coefficient and  $\xi_L$  is the correlation length for the polymer chains (which gives an indication of the gel's mesh size).

The unified model considers that, for each individual level, the scattering intensity is the sum of a Guinier term and a power-law function:

$$I(q) = \sum_{i=1}^N G_i \exp\left(-q^2 \cdot \frac{R_{g,i}^2}{3}\right) + \frac{B_i [\text{erf}(qR_{g,i}/\sqrt{6})]^{3p_i}}{q^{p_i}} + bkg \quad (2)$$

$G_i = c_i V_i \Delta SLD_i^2$  is the exponential pre-factor (where  $V_i$  is the volume of the particle and  $\Delta SLD_i$  is the scattering length density (SLD) contrast existing between the  $i$ th structural feature and the surrounding solvent),  $R_{g,i}$  is the radius of gyration describing the average size of the  $i$ th level structural feature and  $B_i$  is a  $q$ -independent prefactor specific to the type of power-law scattering with power-law exponent,  $p_i$ .

The obtained values from the fitting coefficients are those that minimize the value of Chi-squared, which is defined as:

$$\chi^2 = \sum \left( \frac{y - y_i}{\sigma_i} \right)^2 \quad (3)$$

where  $y$  is a fitted value for a given point,  $y_i$  is the measured data value for the point and  $\sigma_i$  is an estimate of the standard deviation for  $y_i$ . The curve fitting operation is carried out iteratively and for each iteration, the fitting coefficients are refined to minimize  $\chi^2$ .

### 2.8. X-ray diffraction (XRD)

The X-ray diffraction (XRD) analysis was conducted using a Bruker diffractometer model D5005, which was equipped with a secondary monochromator and a Cu tube. The experimental setup employed a  $\theta$ - $2\theta$  configuration, with the samples examined within the angular range of 3°–60°. Each measurement step had a precision of 0.02°, and a count

time of 200 s was allocated per step. Peak fitting of the XRD data was performed utilizing the Igor software package (Wavemetrics, Lake Oswego, Oregon), following the same procedure outlined in a previous study (Martínez-Sanz, Gómez-Mascaraque, et al., 2019). The obtained fitting coefficients were determined by minimizing the value of Chi-squared according to Eq. (4):

$$\chi^2 = \sum \left( \frac{y - y_i}{\sigma_i} \right)^2 \quad (4)$$

In this equation,  $y$  represents the fitted value for a given point,  $y_i$  corresponds to the measured data value for that point, and  $\sigma_i$  is an estimate of the standard deviation for  $y_i$ .

The iterative curve fitting process involved refining the fitting coefficients in each iteration to minimize  $\chi^2$ . From the obtained fitting results, the crystallinity index was determined using Eq. (5):

$$X_C(\%) = \frac{\sum A_{Crystall}}{A_{Total}} \times 100 \quad (5)$$

Where  $A_{Total}$  represents the sum of the areas under all the diffraction peaks, and  $\sum A_{Crystall}$  corresponds to the sum of the areas corresponding to the crystalline peaks.

## 2.9. Texture profile analysis (TPA)

The textural properties of agar-based hydrogels were assessed at ambient conditions using a universal test Machine (Instron, USA) equipped with a cylindrical aluminium plunger (diameter: 3.6 cm) and a 30 N load cell. Gel disk samples were compressed twice with a 50% deformation ratio, while pre-test, test, and post-test speeds were maintained at 1 mm/s. The tiger force, tiger distance, and time interval between bites were set at 5 g, 2 mm, and 50 s, respectively. Each formulation underwent at least three independent measurements. The TPA curves provided information on the mechanical parameters, including hardness (N), which indicates the maximum force required to compress the sample for the first time, and cohesiveness, which is the ratio of positive force during the second compression cycle to that of the first.

## 2.10. Oscillatory rheological measurements

Rheological measurements were carried out using a HR-20 rheometer from TA Instruments (Crawley, England). The cone-plate geometry employed had a diameter of 4 cm, 2° angle, and 53  $\mu$ m gap. To regulate the temperature, a Peltier plate was used, and the cone was equipped with a solvent trap and an evaporation blocker from TA Instruments. Additionally, the samples were coated with a layer of paraffin oil. The hot solutions were freshly prepared and loaded onto the pre-heated rheometer plate at 90 °C. Following a 3-min equilibration period, the temperature was gradually reduced from 90 °C to 20 °C at a constant rate of 2 °C/min, then held at 20 °C for 5 min, and finally increased back to 90 °C. The storage ( $G'$ ) and loss ( $G''$ ) moduli were measured as a function of temperature at a strain of 0.1% and a frequency of 6.28 rad/s, within the linear viscoelastic region.

## 2.11. Uniaxial compression

An Instron universal testing machine (Instron, USA), equipped with a cylindrical aluminium plunger with a diameter of 3.6 cm and a 30 N load cell, was utilized to carry out uniaxial compression tests under ambient conditions. Gel disk specimens were compressed to 90% of their original height at a crosshead speed of 1 mm/s. True stress ( $\sigma_T$ ) and true strain ( $\epsilon_T$ ) were determined from the force (N) and distance (mm) using Eqs. (6) and (7), respectively:

$$\sigma_T = \frac{F(t)(h_0 - \Delta h(t))}{\pi r^2 h_0} \quad (6)$$

$$\epsilon_T = \ln \frac{h_0}{h_0 - \Delta h(t)} \quad (7)$$

where  $F(t)$  is the force,  $\Delta h(t)$  is the change in the height during compression,  $h_0$  is the initial height of the sample and  $r$  is the initial radius of the sample.

Compression moduli were calculated from the slopes of the initial linear zone of the true stress vs. true strain curves. The measurements were performed at least in triplicate.

## 2.12. Optical microscopy

The agar-based hydrogels were subjected to analysis using optical microscopy. Images were captured employing a Nikon Eclipse 90i microscope equipped with a 5-megapixel Nikon Digital Sight DS-5Mc cooled digital colour microphotography camera (Nikon Corporation, Japan). Additionally, images of the materials were obtained using a fluorescent filter UV-2A (Excitation 330–380 nm, Dichroic Mirror 400, and LongPass 420 nm for emission). The acquired pictures were subsequently analysed and processed using Nis-Elements Br 3.2 Software (Nikon Corporation, Japan).

## 2.13. Statistics

All data were represented using the average  $\pm$  standard deviation. Significant differences in both graphs and tables were denoted by different letters ( $p \leq 0.05$ ). The analysis of variance (ANOVA) was conducted followed by a Tukey-test.

# 3. Results and discussion

## 3.1. Composition of the agar-based extracts

Agar-based fractions from three different agarophytes, namely *Gelidium corneum*, *Agarophyton chilensis*, and *Gracilariopsis longissima*, were obtained using two different extraction protocols. A simplified hot water extraction protocol was applied to obtain less purified agar-based fractions. Furthermore, the impact of an initial alkaline pre-treatment step to remove impurities from the raw seaweeds, similar to that used in the agar extraction industry, was evaluated. According to the results presented in Table 1, the extraction yields for HW-G, HW-L, HW-C, NaOH-G, NaOH-L, and NaOH-C were  $10.9 \pm 0.3\%$ ,  $25.6 \pm 4.1\%$ ,  $26.0 \pm 1.1\%$ ,  $3.5 \pm 0.3\%$ ,  $3.9 \pm 0.3\%$ , and  $6.8 \pm 0.7\%$ , respectively. This indicates that, as expected, the purification process negatively affected the extraction yields, which decreased from 3- to 7-fold. This observation is consistent with a previous study, which also involved the extraction of agar fractions from *G. corneum*, in which the application of an alkaline pre-treatment led to a 4-fold decrease in the extraction yield (Martínez-Sanz, Gómez-Mascaraque, et al., 2019). It is also noteworthy that the extraction yields significantly increased for the less purified agar-based fractions obtained from the *Gracilariales* as compared to that obtained from *G. corneum*. Owing to the extensive range of reported extraction parameters, it is difficult to make direct comparisons with previous studies. Nonetheless, high extraction yields have been reported for *Gracilaria* species, with up to 55% yields reported for agars from *Gracilaria cliftonii* produced under conditions similar to those employed in this study (Kumar & Fotedar, 2009).

The composition of the agar-based extracts is compiled in Table 1. The first clear observation is that, as expected, the alkali pre-treatment yielded extracts with higher polysaccharide contents, while other components (especially proteins and ashes) were present in greater amounts in the corresponding extracts produced by omitting the pre-treatment



**Table 1**

Extraction yield, macronutrient composition, antioxidant capacity and sulphur content (S) of the agar-based fractions.

	Extraction yield (%)	Carbohydrate (%)		Protein (%)	Lipid (%)	Ash (%)	Polyphenol (mg GAE/g sample)	Antioxidant capacity ABTS (mg TE/g sample)	S (%)
		Agar <sup>a</sup> (%)	Glucose (%)						
HW-G	10.9 ± 0.3 <sup>c</sup>	56 ± 10.4 [97] <sup>a</sup>	3.5 ± 1 <sup>b</sup>	18.2 ± 1.4 <sup>c</sup>	0.3 ± 0.01 <sup>a</sup>	23.6 ± 1.1 <sup>d</sup>	8.9 ± 1.8 <sup>d</sup>	6.7 ± 0.07 <sup>c</sup>	3.2 ± 0.02 <sup>e</sup>
HW-L	25.6 ± 4.1 <sup>d</sup>	54.4 ± 1.5 [71] <sup>a</sup>	9.7 ± 0.6 <sup>c</sup>	13.7 ± 0.04 <sup>d</sup>	4.7 ± 0.02 <sup>c</sup>	8.5 ± 1.5 <sup>a</sup>	6.2 ± 1.0 <sup>c</sup>	6.0 ± 0.06 <sup>c</sup>	2.1 ± 0.003 <sup>d</sup>
HW-C	26.0 ± 1.1 <sup>d</sup>	59.8 ± 3.7 [82] <sup>a</sup>	2.4 ± 0.03 <sup>a</sup>	8.8 ± 0.1 <sup>c</sup>	4.5 ± 0.08 <sup>c</sup>	16.8 ± 0.2 <sup>c</sup>	4.5 ± 0.4 <sup>b</sup>	6.4 ± 0.07 <sup>d</sup>	2.1 ± 0.014 <sup>d</sup>
NaOH-G	3.5 ± 0.3 <sup>a</sup>	72.0 ± 2.9 [94] <sup>b</sup>	4.7 ± 0.6 <sup>c</sup>	2.2 ± 0.02 <sup>a</sup>	–	9.6 ± 0.9 <sup>ab</sup>	2.6 ± 0.2 <sup>a</sup>	3.9 ± 0.07 <sup>b</sup>	0.3 ± 0.05 <sup>b</sup>
NaOH-L	3.9 ± 0.3 <sup>a</sup>	75.1 ± 8.8 [75] <sup>b</sup>	3.2 ± 0.7 <sup>ab</sup>	2.7 ± 0.2 <sup>a</sup>	3.7 ± 0.2 <sup>b</sup>	7.7 ± 0.4 <sup>a</sup>	2.7 ± 0.1 <sup>a</sup>	3.5 ± 0.2 <sup>a</sup>	0.2 ± 0.007 <sup>a</sup>
NaOH-C	6.8 ± 0.7 <sup>b</sup>	73.3 ± 2.7 [77] <sup>b</sup>	4.9 ± 0.1 <sup>b</sup>	6.6 ± 0.08 <sup>b</sup>	3.7 ± 0.3 <sup>b</sup>	9.1 ± 0.6 <sup>ab</sup>	3.3 ± 0.06 <sup>ab</sup>	7.1 ± 0.09 <sup>f</sup>	0.4 ± 0.007 <sup>c</sup>

Values with different letters are significantly different ( $p \leq 0.05$ ).<sup>a</sup> The value in brackets corresponds to the percentage purity in agarose of each agar fraction as determined by HPAEC-PAD after reductive hydrolysis.

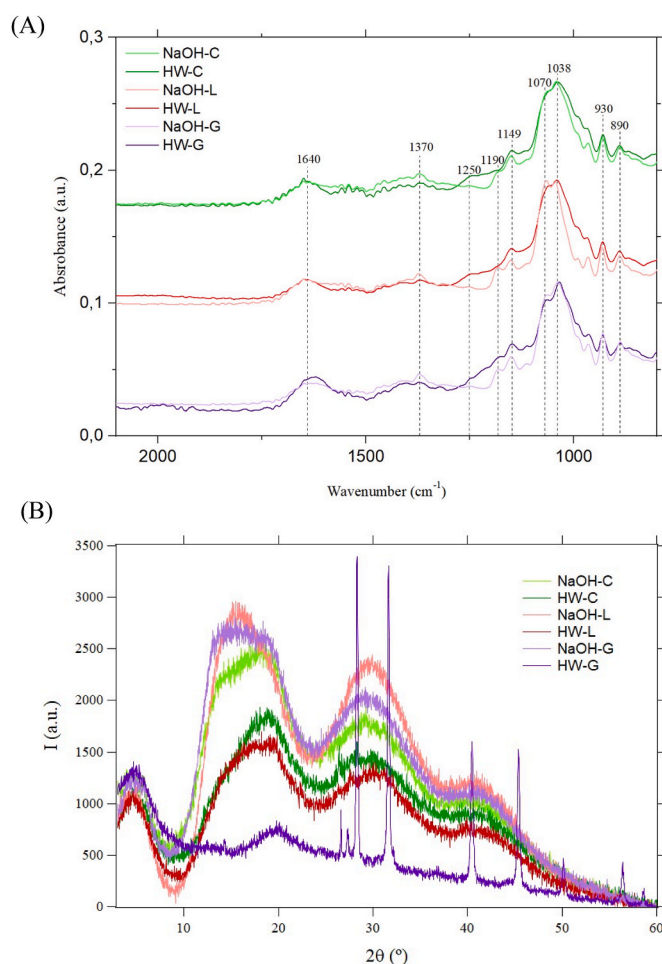
step. In particular, the total carbohydrate content increased from 60 to 64% up to 77–81% when applying the alkaline pre-treatment. Despite their lower carbohydrate content, the HW-G, HW-L and HW-C extracts had a relatively high agar contribution of more than 84% of the total carbohydrates. Surprisingly, the agarose proportion in the agar fraction did not increase with the alkaline pre-treatment. This indicates that the pre-treatment was mainly effective in removing components other than polysaccharides, but did not modify the agarose/agaropectin proportion in the agar. It is also noteworthy that all samples contained glucose, which is likely due to the presence of floridean starch, a storage polysaccharide that may be co-extracted with agar (Carmona, Vergara, Lahaye, & Niell, 1998; Martínez-Sanz, Ström, et al., 2020). In particular, HW-L presented the highest amount of glucose, suggesting that a greater proportion of starch was co-extracted with agar. Although the antioxidant capacity of all agar-based fractions decreased with increasing purification levels, the NaOH-L extract did not exhibit this trend. All samples presented values that were within the range reported for agar fractions extracted from *G. corneum* under similar conditions (Martínez-Sanz et al., 2021; Martínez-Sanz, Gómez-Mascaraque, et al., 2019). Typically, the antioxidant capacity of seaweed-derived compounds is attributed to the presence of phenolic compounds. However, in this case, other bioactive compounds, such as sulphated polysaccharides (e.g. agaropectin) and lipids, may also contribute to the antioxidant capacity, as previously reported (Cebrián-Lloret, Martínez-Abad, López-Rubio, & Martínez-Sanz, 2022).

Interestingly, a clear difference was observed between the composition of the less purified fractions obtained from *G. corneum* and those from *Gracilariales*, since HW-G had the highest protein (18%), ash (24%) and polyphenol (1%) contents, while HW-C and HW-L had higher lipid contents (>4.5%). The protein and ash contents of HW-G were slightly different to those previously reported for agar-based fractions obtained from *G. corneum* using a similar extraction protocol (Martínez-Sanz et al., 2021; Martínez-Sanz, Ström, et al., 2020), which can be due to the impact of seasonal variation on the composition of the raw seaweeds. Another interesting observation is that the agar fractions extracted from *G. corneum* consisted of more than 94% agarose; in contrast, the fractions obtained from species of the *Gracilaria* genera contained less than 82% agarose. This indicates a higher agaropectin content in the fractions extracted from *Gracilariales*, which is expected to have an impact on their gelling behaviour. Surprisingly, despite their lower agarose proportion, the amount of sulphur in the HW-L and HW-C extracts was lower than in HW-G. Although sulphate groups in agar are typically associated to agaropectin, these results suggest that the agaropectin fractions from the *Gracilaria* and *Gelidium* species present different molecular structures, having the agaropectin from *Gracilaria* seaweeds lower degree of sulphate substitution.

It should also be noted that the mass balance was close to 100% for

most of the samples, except for the NaOH-G extract, which accounted for a total of ca. 88%. This discrepancy could be attributed to the considerable agarose content present in this sample, which may be less susceptible to the hydrolysis process used to determine the carbohydrate content, leading to an underestimation of the total carbohydrate content.

The FT-IR spectra of agar-based extracts were recorded to identify their main compositional differences (Fig. 1A). As observed, all samples exhibited a pronounced band at 1038 cm<sup>-1</sup>, which is common to all

**Fig. 1.** (A) FT-IR spectra and (B) XRD patterns from the agar-based fractions.

polysaccharides and is primarily attributed to the coupling of C–O or C–C stretching modes with C–OH bending modes (Guerrero, Etxabide, Leceta, Peñalba, & De La Caba, 2014). The most characteristic agar bands, such as that located at  $890\text{ cm}^{-1}$ , attributed to the C–H of residual  $\beta$ -galactose carbons (Guerrero et al., 2014; Martínez-Sanz, Gómez-Mascaraque, et al., 2019; Martínez-Sanz, Martínez-Abad, & López-Rubio, 2019) as well as those at  $930$  and  $1070\text{ cm}^{-1}$ , associated with the 3,6-anhydro-galactose bridges (Freile-Pelegrín et al., 2007; Guerrero et al., 2014), although present in all fractions, were more evident in the purified extracts, demonstrating the effectiveness of the purification process. Several peaks associated with the vibration of sulphate groups were also observed in the samples such as the peak centred at  $1149\text{ cm}^{-1}$ , present in all samples, or the peak at  $1370\text{ cm}^{-1}$ , which was more pronounced in the purified fractions. Also associated with the vibration of the sulphate groups are the band centred at  $1250\text{ cm}^{-1}$ , which disappeared almost completely in the purified fractions, or the peak centred at  $1190\text{ cm}^{-1}$  which was present in both the purified fractions and the less purified HW-G fraction. Generally, the sulphate group-associated peaks seemed to be more prominent in the fractions obtained from *G. corneum*, consistent with the results from the compositional characterization. This is of particular interest since the presence

of 6-sulphate- $\alpha$ -l-galactose units has been reported to decrease the gel strength of agars (Freile-Pelegrín et al., 2007; Nishinari & Fang, 2017). Finally, the higher protein content in the HW-G fraction was consistent with the greater intensity of the amide I band at  $1640\text{ cm}^{-1}$  (Guerrero et al., 2014) when compared to the other samples.

The crystallinity of the different agar-based fractions was calculated from the XRD patterns of the samples, which are shown in Fig. 1B. As observed, all the samples presented diffraction patterns characteristic of semi-crystalline materials. HW-G displayed a pattern similar to that previously reported for agars extracted from *G. corneum* (Martínez-Sanz, Gómez-Mascaraque, et al., 2019; Rhim, Wang, & Hong, 2013, 2014), where two main diffraction peaks centred at ca.  $13$ – $14^\circ$  and  $19.6^\circ$ , corresponding to the crystalline fraction of agarose, were combined with multiple sharp peaks, arising from the presence of mineral compounds which are found in the raw seaweed, such as silica ( $\text{SiO}_2$ ) and weddellite ( $\text{CaC}_2\text{O}_4 \cdot 2\text{H}_2\text{O}$ ) (Y. W. Chen, Lee, Juan, & Phang, 2016; Singh, Gaikwad, Park, & Lee, 2017). These peaks arising from minerals were not detected in HW-L and HW-C, which is probably due to a lower proportion of this type of compounds in the corresponding seaweeds (Cebrián-Lloret, Martínez-Abad, et al., 2022). After the alkaline pre-treatment, these peaks were also absent in NaOH-G, confirming the efficiency of the

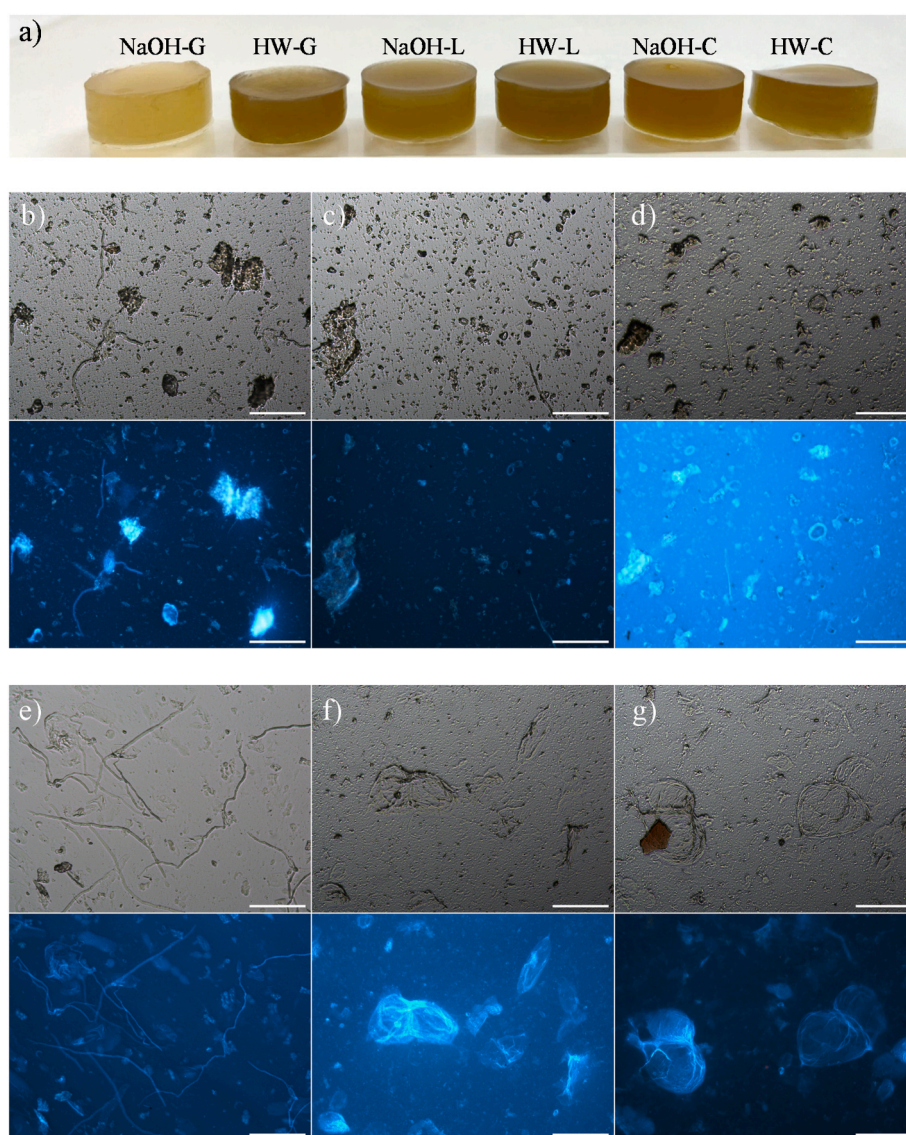


**Fig. 2.** Visual appearance (a) and optical microscopy images (b–g) of the agar-based hydrogels from HW-G (b), HW-L (c), HW-C (d), NaOH-G (e), NaOH-L (f), NaOH-C (g). Scale bars correspond to  $100\text{ }\mu\text{m}$ . Top images were taken with bright light while bottom images were taken using a fluorescent filter UV-2A.



process to remove impurities. The crystallinity indexes were significantly increased from 13% for HW-G, 40% for HW-L and 36% for HW-C, to 78% for NaOH-G, 82% for NaOH-L and 72% for NaOH-C. This agrees with the increase in the polysaccharide content produced by applying the pre-treatment step, which removed more amorphous components such as proteins and non-crystalline ashes. Interestingly, the higher agarose proportion in the agar-based extracts from *G. corneum* did not have a significant impact on the crystallinity, hence suggesting that the agaropectin fraction present in the *Gracilariales* might also be arranged in an ordered conformation, giving rise to the formation of crystalline domains. This might be directly related to the lower degree of sulphate substitution in the agaropectin from these seaweeds.

### 3.2. Structural and functional properties of the agar-based hydrogels

To assess the potential of the agar-based fractions as gelling agents in the food industry, hydrogels were generated, and their functional properties were characterized. The visual appearance of the resulting hydrogels is shown in Fig. 2 (a). As expected, all the samples exhibited a brownish coloration, attributed to the diverse array of compounds present in the extracts. However, the more purified fractions, particularly NaOH-G, showed a lower degree of coloration compared to the other fractions probably due to its lower concentration of polyphenols and proteins. The hydrogels' microstructure was also investigated using optical microscopy and representative images captured in brightfield and under ultraviolet filter are presented in Fig. 2(b–g). The images obtained in brightfield revealed clear changes in the hydrogel structure, both among different seaweed species and with different degrees of purification. In hydrogels prepared from less purified agar fractions, the presence of impurities in the form of non-solubilised cellular tissues was primarily observed. However, these insoluble impurities were mostly removed in the alkali-treated fractions. For the purified agar fractions, the hydrogels clearly showed distinct microstructures depending on the seaweed species of origin. Specifically, the hydrogels from *G. corneum* were characterized by the presence of fibrillar structures, while those from *Gracilariales* species exhibited globular structures. When observing the images captured under the UV filter, it is noticeable that both the cellular structures found in hydrogels prepared from less purified fractions and the fibres and globular structures observed in hydrogels from pure fractions exhibited a bright blue fluorescence. As previously indicated (Cebrián-Lloret, Martínez-Abad, et al., 2022), these fluorescent regions are likely indicative of agar-rich areas. The greater proportion of agarose in the NaOH-G extract, which is known to form double helices which then aggregate into larger bundles (Dai & Matsukawa, 2013; Descallar & Matsukawa, 2020), may be responsible for the observed fibrillar structures. In contrast, the presence of semi-crystalline agaropectin in the *Gracilariales* may have given rise to the formation of globular structures.

The mechanical properties of the agar-based hydrogels were assessed by means of compression tests and the most representative parameters, i. e. Young's modulus ( $E$ ) and maximum stress ( $\sigma_{\max}$ ), obtained from the stress–strain curves (cf. Fig. S1 from the Supplementary Material) are summarized in Table 2. As expected, the presence of other compounds in the less purified fractions resulted in hydrogels that showed less stiff

behaviour within the linear elastic region and less resistance to fracture during compression. Notably, amongst the less purified fractions, HW-G yielded stiffer and stronger gels compared to the other two fractions. This could be attributed to the higher agarose proportion in the agar from this extract, since several studies have reported that agarose is the main fraction responsible for the formation of strong hydrogel networks (Martínez-Sanz, Ström, et al., 2020; Nishinari & Fang, 2017; Zarrintaj et al., 2018). Nonetheless, the higher protein content of HW-G could also be playing an important role on its mechanical performance, as previous studies have shown that agar can interact via hydrogen bonds with proteins to form a network with enhanced physicochemical properties (Garrido, Etxabide, Guerrero, & De La Caba, 2016; Gupta & Nayak, 2015). In the case of the hydrogels produced from the purified fractions, those obtained from the *Gracilariales* exhibited the highest Young's modulus and tensile strength, with the NaOH-L fraction demonstrating slightly superior stiffness of 27 kPa and a maximum strain of 4.7 kPa. These values fall within the range previously reported for commercial agar hydrogels (Martínez-Sanz, Ström, et al., 2020; Ross, Pyrak-Nolte, & Campanella, 2006; Sharma & Bhattacharya, 2014), demonstrating that *Gracilariopsis longissima* is a cost-effective alternative to traditional agar sources for obtaining high-stiffness hydrogels. The slightly superior mechanical performance of the hydrogels from *Gracilariales* might be attributed to (i) the presence of a semi-crystalline agaropectin network, capable of strengthening the agarose gelling network and/or (ii) a beneficial effect of small amounts of other components such as proteins, lipids and polyphenols, capable of interacting with agar and contributing to the formation of stronger networks.

TPA analyses were also performed on the agar-based hydrogels, and the curves provided information on relevant mechanical parameters, including hardness ( $N$ ) and cohesiveness. The results obtained are compiled in Table 2. As anticipated, the more purified agar samples exhibited higher hardness, which is related to the gel strength. Specifically, the NaOH-L hydrogel had the highest hardness (ca. 29  $N$ ), followed by NaOH-G (ca. 22  $N$ ) and NaOH-C (ca. 13  $N$ ), in accordance with the results obtained from the compression tests. In contrast, the presence of other compounds in the less purified agar samples led to gels with lower toughness, yet, in the case of the HW-L and HW-C hydrogels, with higher cohesiveness. This latter parameter is a measure of a gel's ability to withstand external damage while retaining its structural integrity, and it is thus indicative of internal binding strength (H. Chen et al., 2021; Fontes-Candia et al., 2022). This higher cohesiveness may be partly attributed to the higher lipid content in these agar-based fractions, as previous studies have reported that an increase in fat content can directly affect the increase of this textural parameter (Badar, Liu, & Xia, 2021, pp. 4739–4778; Fontes-Candia et al., 2023). Other factors, such as degree of sulphation or the different composition of the extracts may also influence the cohesiveness values.

In order to investigate the influence of the composition on the gelling mechanism of the agar-based extracts, oscillatory rheological tests were conducted. The elastic ( $G'$ ) and viscous ( $G''$ ) moduli were recorded during cooling and heating ramps, and the results are presented in Fig. 3. During the cooling phase, all samples exhibited similar behaviour, showing an initial stage in which  $G'$  and  $G''$  remained relatively constant, followed by a sharp increase in both moduli as the temperature decreased below a certain value, and a final stage in which both moduli reached a plateau or continued to increase slowly. The gelation temperature of agars has been frequently estimated from the crossover point of  $G'$  and  $G''$  during cooling ramps. However, except for samples HW-L and HW-C, for which the crossover point was detected at 42.2 °C and 39.4 °C respectively, none of the other samples exhibited true solution behaviour ( $G'' > G'$ ). Instead, they showed a behaviour typical of solid-like entangled networks at the initial temperature of 75 °C, similarly to that previously observed for agar fractions obtained from *G. corneum* (Martínez-Sanz, Ström, et al., 2020). Since no true crossover between  $G'' > G'$  was observed, in line with other previous studies (Alehosseini et al., 2018; Martínez-Sanz, Ström, et al., 2020), the apparent gelation

**Table 2**  
Mechanical properties of the agar-based hydrogels.

	$E$ (kPa)	$\sigma_{\max}$ (kPa)	Hardness (N)	Cohesiveness
HW-G	11.2 ± 0.9 <sup>b</sup>	2.0 ± 0.07 <sup>c</sup>	1.1 ± 0.1 <sup>a</sup>	2.9 ± 0.4 <sup>a</sup>
HW-L	5.9 ± 0.3 <sup>a</sup>	1.0 ± 0.02 <sup>b</sup>	6.4 ± 0.3 <sup>c</sup>	7.6 ± 2.5 <sup>b</sup>
HW-C	4.1 ± 1.7 <sup>a</sup>	0.3 ± 0.02 <sup>a</sup>	3.6 ± 0.2 <sup>b</sup>	8.8 ± 1.8 <sup>b</sup>
NaOH-G	22.3 ± 1.5 <sup>c</sup>	3.3 ± 0.3 <sup>d</sup>	21.8 ± 2.2 <sup>e</sup>	3.5 ± 0.2 <sup>a</sup>
NaOH-L	27.5 ± 1.3 <sup>d</sup>	4.7 ± 0.1 <sup>f</sup>	29.2 ± 1.6 <sup>f</sup>	3.6 ± 0.1 <sup>a</sup>
NaOH-C	26.7 ± 0.9 <sup>d</sup>	4.1 ± 0.04 <sup>e</sup>	13.0 ± 1.1 <sup>d</sup>	3.8 ± 0.4 <sup>a</sup>

Values within the same column with different letters are significantly different ( $p \leq 0.05$ ).

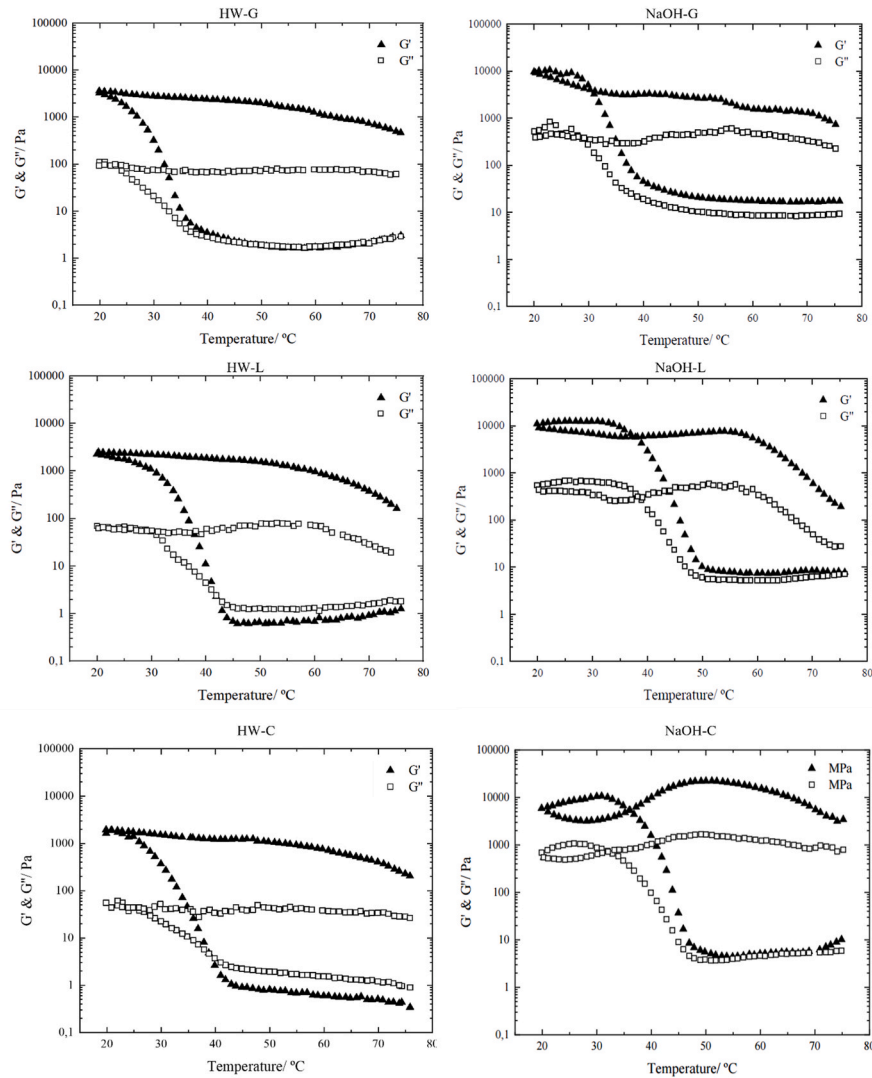


Fig. 3. Temperature dependence of  $G'$  (filled triangles) and  $G''$  (open squares) moduli of agar-based extracts during cooling and heating ramps.

temperature was defined by determining the point at which there was an abrupt increase in  $G'$  and  $G''$ . As shown in Table 3, this transition occurred in the 37–42 °C range for all the less purified extracts, as well as the purified NaOH-G extract, which is consistent with the range of gelation temperatures commonly reported in the literature for agar samples (40–10 °C) (Martínez-Sanz, Ström, et al., 2020; Rocha et al., 2019). This may suggest that the presence of other components, such as ashes or proteins, in the less purified extract from *G. corneum*, did not have a strong impact on the temperature at which agarose helices aggregated to form hydrogels, in line with previous studies

Table 3

Rheological and mechanical properties of the different agar-based extracts: Apparent gelation temperature ( $T_g$ ), elastic modulus ( $G'_{20^\circ\text{C}}$ ), viscous modulus ( $G''_{20^\circ\text{C}}$ ) and  $\tan \delta$  measured at 20 °C.

	$T_g$ (°C)	$G'_{20^\circ\text{C}}$ (kPa)	$G''_{20^\circ\text{C}}$ (kPa)	$\tan \delta$
HW-G	$37.8 \pm 0.07^a$	$3.6 \pm 0.4^b$	$0.12 \pm 0.02^b$	$0.03 \pm 0.002^a$
HW-L	$42.2 \pm 0.1^d$	$2.3 \pm 0.006^a$	$0.08 \pm 0.02^{ab}$	$0.04 \pm 0.006^a$
HW-C	$39.4 \pm 0.03^c$	$1.5 \pm 0.1^a$	$0.05 \pm 0.01^a$	$0.04 \pm 0.01^a$
NaOH-G	$38.5 \pm 0.1^b$	$8.6 \pm 0.7^d$	$0.5 \pm 0.01^c$	$0.06 \pm 0.008^a$
NaOH-L	$48.4 \pm 0.4^e$	$10.5 \pm 0.3^e$	$0.6 \pm 0.08^d$	$0.05 \pm 0.008^a$
NaOH-C	$48.2 \pm 0.07^e$	$5.1 \pm 1.1^c$	$0.7 \pm 0.003^d$	$0.11 \pm 0.04^b$

Values within the same column with different letters are significantly different ( $p \leq 0.05$ ).

(Martínez-Sanz, Ström, et al., 2020). In contrast, the more purified extracts obtained from *Gracilariales* showed higher gelation temperatures (ca. 48 °C) than those of their corresponding less purified extracts. This is consistent with previous findings showing that high gelation temperatures are common in agars obtained from *Gracilaria* spp., particularly if they are highly methylated (Rocha et al., 2019) and might indicate that, when reducing the amount of other components, the agaroprotein present in these seaweeds is capable of forming a strong gelling network along with the agarose. The elastic modulus ( $G'$ ) is a measure of the solid nature of a sample and is expected to be positively correlated with gel strength. In fact, the values for  $G'$  at 20 °C followed a similar trend to those from the gel strength, being the highest in the more purified agars, particularly in the NaOH-L hydrogel (ca. 11 kPa), followed by NaOH-G (ca. 9 kPa) and NaOH-C (ca. 5 kPa). Furthermore, the presence of other compounds in the less purified fractions negatively affected the elastic modulus of the hydrogels, consistent with the results obtained during mechanical testing. However, several authors have also reported values similar to those obtained in this study for agars obtained from different agarophyte species (Bertasa et al., 2020; Rocha et al., 2019). In contrast,  $\tan \delta$  values ( $\tan \delta = G''/G'$ ) were similar for all the samples (approximately 0.03–0.11), indicating a comparable amount of elastic response.

The nanostructure of the agar-based gels was investigated by means of SAXS and the obtained scattering patterns are shown in Fig. 4. The



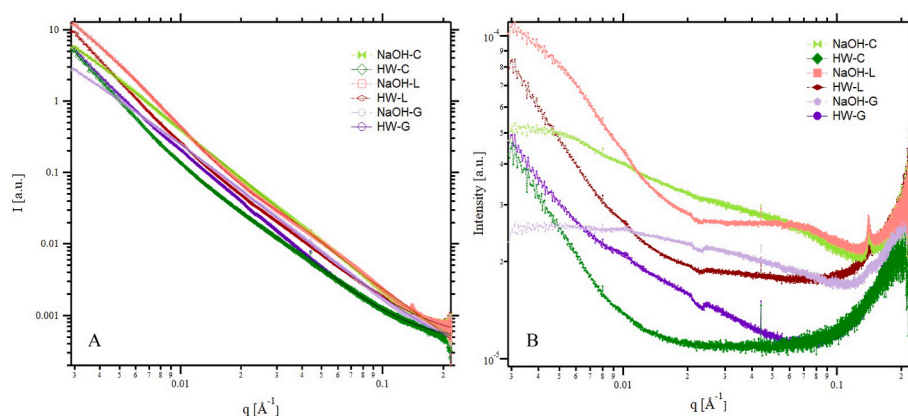


**Fig. 4.** (A) SAXS patterns and (B) corresponding Kratky plots from the agar-based hydrogels. In (A) markers represent the experimental data and solid lines show the fits obtained using the corresponding fitting models.

scattering data from most of the samples could be fitted using a simple correlation length model, while in the case of the NaOH-L hydrogel, given the appearance of two obvious shoulder-like features (which are more clearly visualized in the Kratky plot, Fig. 4B), a unified model with two structural levels produced much better fit to the experimental data (see the obtained parameters in Table S1). For the less purified agars, the power-law exponents were close to 3, indicating the existence of clustered networks formed by the association of the agarose double helices to form the gelling networks, while the Lorentzian exponents, close to 2, were indicative of polymeric chains with a random coil conformation. The correlation length, which can be related to the size of the agarose double helices, was ca. 5 nm for HW-L and HW-C, while it was ca. 12 nm for HW-G. This is in agreement with the higher agarose content in HW-G, hence facilitating the formation of larger aggregates upon gelation, in line with previous work (Martínez-Sanz, Ström, et al., 2020). The alkaline pre-treatment led to the formation of larger agarose bundles, as evidenced by the greater correlation lengths for NaOH-G (ca. 26 nm) and NaOH-C (ca. 53 nm). In the particular case of the NaOH-L hydrogel, the applied unified model suggested the existence of two different structural levels. One of them might be related to the individual agarose double helices (ca. 4 nm) and the other one might be attributed to the formation of larger aggregates or bundles of double helices (ca. 53 nm). The existence of thicker agarose bundles or aggregates in alkali-treated agar hydrogels has been previously noted and has been related to the greater agar purity obtained after applying the pre-treatment (Martínez-Sanz, Ström, et al., 2020). The fact that larger aggregates seemed to be present in the NaOH-L and NaOH-C can explain the superior mechanical and rheological properties of these hydrogels as compared with NaOH-G and might be explained by the semi-crystalline character of the less sulphated agaropeptins present in the *Gracilariiales* species, which could be interacting with agarose to form thicker bundles. It should also be noted that the NaOH-L and NaOH-C hydrogels presented a small sharp peak at  $0.14 \text{ \AA}^{-1}$ , corresponding to a real distance of ca. 4.5 nm. A similar peak has been reported to appear in cellulose-based hydrogels (Martínez-Sanz, Lopez-Sanchez, Gidley, & Gilbert, 2015), corresponding to the centre-to-centre distance from the tightly packed cellulose microfibrils. The fact that this peak was visible in these agar-based hydrogels indicates the existence of highly ordered structures, most likely formed by tightly packed agarose/agaropeptin double helices. Once again, this provides evidence for the formation of more densely packed hydrogel networks in the case of NaOH-L and NaOH-C and, thus, confirms that these two *Gracilariiales* could be used to produce agars with superior mechanical performance to that from *G. corneum*, provided that an alkaline pre-treatment is applied.

#### 4. Conclusions

The aim of this work was to compare the composition and gelling behaviour of agar fractions obtained from different red seaweed species, using both conventional and alternative extraction methods, hence assessing their appropriateness for use in the food industry. The different seaweeds used comprised two species commonly used for agar extraction (*Gelidium corneum* and *Agarophyton chilensis*) and a more inexpensive species that is not typically employed for this purpose (*Gracilariopsis longissima*). The results of this study indicate that the conventional alkaline purification process had a detrimental impact on the extraction yield, which decreased by up to four-fold, but produced extracts with a greater carbohydrate content, by removing other components such as proteins, lipids, and ashes. In turn, the agarose/agaropeptin ratio in the agar fraction was not affected by the pre-treatment. Despite the presence of these compounds in the less purified agar fractions, the gelation temperature was not affected, but the hydrogels presented a less rigid behaviour and lower fracture toughness than their more purified counterparts. Surprisingly, the purified fractions from the *Gracilariiales*, particularly NaOH-L, exhibited greater gel strength and toughness, and displayed a higher gelation temperature ( $48^\circ\text{C}$ ), than the purified fraction from *G. corneum*. This was attributed mainly to the presence of agaropeptin with a lower degree of sulphation in the *Gracilariiales*, which presented a semi-crystalline structure and seemed to interact with the agarose fraction to form thicker bundles of double helices, hence strengthening the hydrogel network.

The more energy-efficient alternative extraction protocol yields less purified agar fractions, containing additional compounds such as proteins, polyphenols, and minerals. This might be advantageous for the production of hydrogels with bioactive properties that may be suited for particular applications in the food industry, such as texture modifiers or thickening agents. Furthermore, this study highlights the potential of *Gracilariopsis longissima* as a cost-effective alternative to traditional agar sources for obtaining high stiffness hydrogels. It should be noted that due to the lack of specific regulations for the human consumption of seaweed-based products, there are still many open questions with regards to the requirements of these type of products for food applications. However, given the emergence of seaweeds as novel food sources, the situation is expected to change over the next few years.

#### Author statement

Vera Cebrián-Lloret: Conceptualization, Data curation, Formal analysis, Investigation, Methodology, Writing - original draft, Writing - review & editing. Antonio Martínez-Abad: Conceptualization, Formal analysis, Funding acquisition, Investigation, Methodology, Resources, Supervision, Writing - review & editing. Amparo López-Rubio:

Conceptualization, Formal analysis, Funding acquisition, Investigation, Methodology, Resources, Supervision, Writing - review & editing. Marta Martínez-Sanz: Conceptualization, Formal analysis, Funding acquisition, Investigation, Methodology, Resources, Supervision, Writing - review & editing.

## Declaration of competing interest

The authors declare that they have no known competing financial interests or personal relationships that could have appeared to influence the work reported in this paper.

## Data availability

Data will be made available on request.

## Acknowledgements

This work was financially supported by Hispanagar. Synchrotron experiments were performed at NCD beamline at ALBA Synchrotron with the collaboration of ALBA staff (proposal 2022025569). The authors also acknowledge funding from the Spanish ministry of Science and Innovation through project PID 2020-117744RJ-I00 and grant CEX 2021-001189-S as well as the European Commission through project CIRCALGAE (Horizon Europe) under grant agreement 101060607.

## Appendix A. Supplementary data

Supplementary data to this article can be found online at <https://doi.org/10.1016/j.foodhyd.2023.109177>.

## References

- Alehosseini, A., Gomez del Pulgar, E. M., Gómez-Mascaraque, L. G., Martínez-Sanz, M., Fabra, M. J., Sanz, Y., et al. (2018). Unpurified Gelidium-extracted carbohydrate-rich fractions improve probiotic protection during storage. *LWT*, 96, 694–703.
- Badar, I. H., Liu, H., & Xia, X. (2021). *Future trends of processed meat products concerning perceived healthiness: A review* (pp. 4739–4778). February.
- Bermejo, R., Macías, M., Sánchez-García, F., Love, R., Varela-Álvarez, E., & Hernández, I. (2020). Influence of irradiance, dissolved nutrients and salinity on the colour and nutritional characteristics of *Gracilariopsis longissima* (Rhodophyta). *Algal Research*, 52, Article 102121.
- Bertaso, M., Doderio, A., Alloisio, M., Vicini, S., Riedo, C., Sansonetti, A., et al. (2020). Agar gel strength: A correlation study between chemical composition and rheological properties. *European Polymer Journal*, 123, Article 109442.
- Carmona, R., Vergara, J. J., Lahaye, M., & Niell, F. X. (1998). Light quality affects morphology and polysaccharide yield and composition of *Gelidium sesquipedale* (Rhodophyceae). *Journal of Applied Phycology*, 10(3), 323–332.
- Cebrián-Lloret, V., Göksen, G., Martínez-Abad, A., López-Rubio, A., & Martínez-Sanz, M. (2022). Agar-based packaging films produced by melt mixing: Study of their retrogradation upon storage. *Algal Research*, 66, Article 102802.
- Cebrián-Lloret, V., Martínez-Abad, A., López-Rubio, A., & Martínez-Sanz, M. (2022). Sustainable bio-based materials from minimally processed red seaweeds: Effect of composition and cell wall structure. *Journal of Polymers and the Environment*, 31(3), 886–899.
- Chen, H., Chen, F., Xiao, Q., Cai, M., Yang, Q., Weng, H., et al. (2021). Structure and physicochemical properties of amphiphilic agar modified with octenyl succinic anhydride. *Carbohydrate Polymers*, 251, Article 117031.
- Chen, Y. W., Lee, H. V., Juan, J. C., & Phang, S. M. (2016). Production of new cellulose nanomaterial from red algae marine biomass *Gelidium elegans*. *Carbohydrate Polymers*, 151, 1210–1219.
- Cong, L., Zou, B., Palacios, A., Navarro, M. E., Qiao, G., & Ding, Y. (2022). Thickening and gelling agents for formulation of thermal energy storage materials – a critical review. *Renewable and Sustainable Energy Reviews*, 155, Article 111906.
- Dai, B., & Matsukawa, S. (2013). Elucidation of gelation mechanism and molecular interactions of agarose in solution by <sup>1</sup>H NMR. *Carbohydrate Research*, 365, 38–45.
- Descallar, F. B. A., & Matsukawa, S. (2020). Change of network structure in agarose gels by aging during storage studied by NMR and electrophoresis. *Carbohydrate Polymers*, 245, Article 116497.
- Fathima, A., Chiome, T. J., Catherine, A. A., Egbuna, C., Achar, R. R., & Srinivasan, A. (2022). Smart use of nanomaterials as sensors for detection and monitoring of food spoilage. In *Application of nanotechnology in food science, processing and packaging*.
- Fontes-Candia, C., Martínez-Sanz, M., Gómez-Cortés, P., Calvo, M. V., Verdú, S., Grau, R., et al. (2023). Polysaccharide-based emulsion gels as fat replacers in Frankfurter sausages: Physicochemical, nutritional and sensorial evaluation. *LWT*, 180, Article 114705.
- Fontes-Candia, C., Martínez, J. C., López-Rubio, A., Salvia-Trujillo, L., Martín-Belloso, O., & Martínez-Sanz, M. (2022). Emulsion gels and oil-filled aerogels as curcumin carriers: Nanostructural characterization of gastrointestinal digestion products. *Food Chemistry*, 387, Article 132877.
- Freile-Pelegrín, Y., Madera-Santana, T., Robledo, D., Veleza, L., Quintana, P., & Azamar, J. A. (2007). Degradation of agar films in a humid tropical climate: Thermal, mechanical, morphological and structural changes. *Polymer Degradation and Stability*, 92(2), 244–252.
- Garrido, T., Etxabide, A., Guerrero, P., & De La Caba, K. (2016). Characterization of agar/soy protein biocomposite films: Effect of agar on the extruded pellets and compression moulded films. *Carbohydrate Polymers*, 151, 408–416.
- Guerrero, P., Etxabide, A., Leceta, I., Peñalba, M., & De La Caba, K. (2014). Extraction of agar from *Gelidium sesquipedale* (Rhodophyta) and surface characterization of agar based films. *Carbohydrate Polymers*, 99, 491–498.
- Gupta, P., & Nayak, K. K. (2015). Characteristics of protein-based biopolymer and its application. *Polymer Engineering & Science*, 55(3), 485–498.
- He, Y., Meda, V., Reaney, M. J. T., & Mustafa, R. (2021). Aquafaba, a new plant-based rheological additive for food applications. *Trends in Food Science & Technology*, 111, 27–42.
- Ilavsky, J., & Jemian, P. R. (2009). Irena: Tool suite for modeling and analysis of small-angle scattering. *Journal of Applied Crystallography*, 42(2), 347–353.
- Jayakody, M. M., Vanniarachchy, M. P. G., & Wijesekara, I. (2022). Seaweed derived alginate, agar, and carrageenan based edible coatings and films for the food industry: A review. *Journal of Food Measurement and Characterization*, 16(Issue 2). Springer US.
- Kartik, A., Akhil, D., Lakshmi, D., Panchamoorthy Gopinath, K., Arun, J., Sivaramakrishnan, R., et al. (2021). A critical review on production of biopolymers from algae biomass and their applications. *Bioresource Technology*, 329, Article 124868.
- Kieffer, J., & Wright, J. P. (2013). PyFAI: A python library for high performance azimuthal integration on GPU. *Powder Diffraction*, 28(SUPPL.2).
- Kumar, V., & Fotedar, R. (2009). Agar extraction process for *Gracilaria cliftonii* (Withell, millar, & Kraft, 1994). *Carbohydrate Polymers*, 78(4), 813–819.
- Lee, W. K., Lim, Y. Y., Leow, A. T. C., Namasivayam, P., Ong Abdullah, J., & Ho, C. L. (2017). Biosynthesis of agar in red seaweeds: A review. *Carbohydrate Polymers*, 164, 23–30.
- Löfgren, L., Ståhlman, M., Forsberg, G. B., Saarinen, S., Nilsson, R., & Hansson, G. I. (2012). The BUMe method: A novel automated chloroform-free 96-well total lipid extraction method for blood plasma. *Journal of Lipid Research*, 53(8), 1690–1700.
- Martínez-Sanz, M., Cebrián-Lloret, V., Mazarro-Ruiz, J., & López-Rubio, A. (2020). Improved performance of less purified cellulosic films obtained from agar waste biomass. *Carbohydrate Polymers*, Article 115887.
- Martínez-Sanz, M., Gomez-Barrio, L. P., Zhao, M., Tiwari, B., Knutsen, S. H., Ballance, S., et al. (2021). Alternative protocols for the production of more sustainable agar-based extracts from *Gelidium sesquipedale*. *Algal Research*, 55, Article 102254.
- Martínez-Sanz, M., Gómez-Mascaraque, L. G., Ballester, A. R., Martínez-Abad, A., Brodtkorb, A., & López-Rubio, A. (2019). Production of unpurified agar-based extracts from red seaweed *Gelidium sesquipedale* by means of simplified extraction protocols. *Algal Research*, 38, Article 101420.
- Martínez-Sanz, M., Lopez-Sanchez, P., Gidley, M. J., & Gilbert, E. P. (2015). Evidence for differential interaction mechanism of plant cell wall matrix polysaccharides in hierarchically-structured bacterial cellulose. *Cellulose*, 22(3), 1541–1563.
- Martínez-Sanz, M., Martínez-Abad, A., & López-Rubio, A. (2019). Cost-efficient bio-based food packaging films from unpurified agar-based extracts. *Food Packaging and Shelf Life*, 21, Article 100367.
- McClements, D. J., & Grossmann, L. (2021). The science of plant-based foods: Constructing next-generation meat, fish, milk, and egg analogs. *Comprehensive Reviews in Food Science and Food Safety*, 20(4), 4049–4100.
- Mouga, T., & Fernandes, I. B. (2022). The red seaweed giant *Gelidium* (*Gelidium corneum*) for new bio-based materials in a circular economy framework. *Earth*, 3(3), 788–813.
- Nishinari, K., & Fang, Y. (2017). Relation between structure and rheological/thermal properties of agar. A mini-review on the effect of alkali treatment and the role of agarpectin. *Food Structure*, 13, 24–34.
- Özçimen, D., Benan, İ., Morkoç, O., & Efe, A. (2017). A review on algal biopolymers (pp. 7–14).
- Pangestuti, R., & Kim, S.-K. (2015). An overview of phycocolloids: The principal commercial seaweed extracts. In *Marine algae extracts* (pp. 319–330).
- Qin, Y., Jiang, J., Zhao, L., Zhang, J., & Wang, F. (2018). Applications of alginate as a functional food ingredient. *Biopolymers for Food Design*, 409–429.
- Quemener, B., & Lahaye, M. (1998). Comparative analysis of sulfated galactans from red algae by reductive hydrolysis and mild methanolysis coupled to two different HPLC techniques. *Journal of Applied Phycology*, 10.
- Re, R., Pellegrini, N., Progettante, A., Pannala, A., Yang, M., & Rice-Evans, C. (1999). Antioxidant activity applying an improved ABTS radical cation decolorization assay. *Free Radical Biology and Medicine*, 26(9), 1231–1237.
- Rhim, J. W., Wang, L. F., & Hong, S. I. (2013). Preparation and characterization of agar/silver nanoparticles composite films with antimicrobial activity. *Food Hydrocolloids*, 32(2), 327–335.
- Rhim, J. W., Wang, L. F., Lee, Y., & Hong, S. I. (2014). Preparation and characterization of bio-nanocomposite films of agar and silver nanoparticles: Laser ablation method. *Carbohydrate Polymers*, 103(1), 456–465.
- Rocha, C. M. R., Sousa, A. M. M., Kim, J. K., Magalhães, J. M. C. S., Yarish, C., & Gonçalves, M. do P. (2019). Characterization of agar from *Gracilaria tikvahiae* cultivated for nutrient bioextraction in open water farms. *Food Hydrocolloids*, 89, 260–271.

- Ross, K. A., Pyrak-Nolte, L. J., & Campanella, O. H. (2006). The effect of mixing conditions on the material properties of an agar gel - microstructural and macrostructural considerations. *Food Hydrocolloids*, 20(1), 79–87.
- Sharma, S., & Bhattacharya, S. (2014). Strain and strain rate dependence of gellan, agar and agar–gellan gels as model systems. *Journal of Food Engineering*, 141, 93–98.
- Singh, S., Gaikwad, K. K., Park, S.-I., & Lee, Y. S. (2017). Microwave-assisted step reduced extraction of seaweed (*Gelidium aceroso*) cellulose nanocrystals. *International Journal of Biological Macromolecules*, 99, 506–510.
- Singleton, V. L., Orthofer, R., & Lamuela-Raventós, R. M. (1999). [14] Analysis of total phenols and other oxidation substrates and antioxidants by means of folin-ciocalteu reagent. In *Methods in enzymology* (Vol. 299, pp. 152–178). Elsevier.
- Stevenson, T. T., & Furneaux, R. H. (1991). Chemical methods for the analysis of sulphated galactans from red algae. *Carbohydrate Research*, 210(C), 277–298.
- Wang, L., Shen, Z., Mu, H., Lin, Y., Zhang, J., & Jiang, X. (2017). Impact of alkali pretreatment on yield, physico-chemical and gelling properties of high quality agar from *Gracilaria tenuistipitata*. *Food Hydrocolloids*, 70, 356–362.
- Wiles, P. G., Gray, I. K., & Kissling, R. C. (1998). Routine analysis of proteins by Kjeldahl and Dumas methods: Review and interlaboratory study using dairy products. *Journal of AOAC International*, 81(3), 620–632. International, C. D. C. E. J. G. K. G. K. H. M. K. K. L. H. M. K. M. A. P. M. R. F. V. M. %J J. of A.
- Williams, P. A., & Phillips, G. O. (2021). *Introduction to food hydrocolloids. Handbook of Hydrocolloids* (pp. 3–26).
- Yarnpakdee, S., Benjakul, S., & Kingwascharapong, P. (2015). Physico-chemical and gel properties of agar from *Gracilaria tenuistipitata* from the lake of Songkhla, Thailand. *Food Hydrocolloids*, 51, 217–226.
- Zarrintaj, P., Manouchehri, S., Ahmadi, Z., Saeb, M. R., Urbanska, A. M., Kaplan, D. L., et al. (2018). Agarose-based biomaterials for tissue engineering. *Carbohydrate Polymers*, 187, 66–84.